Biomaterials 293 (2023) 121984

Contents lists available at ScienceDirect

Biomaterials

journal homepage: www.elsevier.com/locate/biomaterials

New vegetable-waste biomaterials by *Lupin albus* L. as cellular scaffolds for applications in biomedicine and food

Silvia Buonvino [a,1], Matteo Ciocci [a,1], Francesca Nanni [b,c], Ilaria Cacciotti [b,d,e], Sonia Melino [a,e,*]

[a] Department of Chemical Sciences and Technologies, NAST Center- University of Rome Tor Vergata, Via della Ricerca Scientifica 1, 00133-Rome, Italy
[b] Italian Interuniversity Consortium on Materials Science and Technology (INSTM), Italy
[c] Enterprise Engineering Department, University of Rome Tor Vergata, Italy
[d] University of Rome "Niccolò Cusano", Engineering Department, Italy
[e] CIMER Center of Regenerative Medicine, University of Rome Tor Vergata, Italy

ARTICLE INFO

Keywords:
Bioplastics
Mesenchymal stem cells
Circular economy
Bioeconomy
Vegetable-patch
Cell-based food

ABSTRACT

The reprocessing of vegetal-waste represents a new research field in order to design novel biomaterials for potential biomedical applications and in food industry. Here we obtained a biomaterial from *Lupinus albus* L. hull (LH) that was characterized micro-structurally by scanning electron microscopy and for its antimicrobial and scaffolding properties. A good adhesion and proliferation of human mesenchymal stem cells (hMSCs) seeded on LH scaffold were observed. Thanks to its high content of cellulose and beneficial phytochemical substances, LH and its derivatives can represent an available source for fabrication of biocompatible and bioactive scaffolds. Therefore, a reprocessing protocol of LH was optimized for producing a new LH bioplastic named BPLH. This new biomaterial was characterized by chemico-physical analyses. The water uptake, degradability and antimicrobial properties of BPLH were evaluated, as well as the mechanical properties. A good adhesion and proliferation of both fibroblasts and hMSCs on BPLH were observed over 2 weeks, and immunofluorescence analysis of hMSCs after 3 weeks indicates an initial commitment toward muscle differentiation. Our work represents a new approach toward the recovery and valorization of the vegetal waste showing the remarkable properties of LH and BPLH as cellular waste-based scaffold with potential applications in cell-based food field as well as in medicine for topical patches in wound healing and bedsores treatment.

1. Introduction

The production of novel stem cell scaffolds able to carefully mimic the biochemical and physical properties of the cellular microenvironment found in tissues and organs is acquiring a considerable importance in regenerative medicine [1–4]. Selected biowastes can represent an inexpensive source of valuable bio-products for the development of innovative sustainable biomaterials for biomedical applications and a new research line on the reuse and renewal of the waste products [5–7]. Improving the waste management could lead to increased opportunities to exploit the bio-wastes and to a reduced environmental impact, also enhancing the competitiveness through the production of new bio-products at lower cost. Recently, micro-structured biomaterials have been used as cell culture systems suitable for preclinical studies on drugs, cytotoxicity analyses and tissue regeneration [8–13]. The complexity of the extracellular matrix (ECM) physiologic microenvironment can be reproduced mimicking its biochemical and physical properties with novel biocompatible micro-structured scaffolds [10].

Abbreviations: α-SMA, α-smooth muscle actin; ATR-FTIR, Attenuated total reflection Fourier transform infrared spectroscopy; BPLH, Bioplastic from lupin hull; DASH, Dietary Approach to Stop Hypertension; DMSO, Dimethyl sulfoxide; ECM, extracellular matrix; FEG, field emission gun; FLH, Fresh lupin hull; GA, Gallic acid; GAE, Gallic acid equivalents; GI, glycemic-index; hMSCs, Lin^{-} $Sca\text{-}1^{+}$ human mesenchymal stem cells; HR, high resolution; IL, interleukin; iPSCs, induced Pluripotent Stem Cells; LH, Lupinus albus hull; MTT, 3-(4,5-dimethyl-2-thiazolyl)-2,5-diphenyl-2H-tetrazolium bromide; Nf-kB, nuclear factor kappa light chain enhancer of activated B cells; NHDFs, Normal human dermal fibroblasts; RH, Relative humidity; RP-HPLC, reverse phase high performance liquid chromatography; SEM, scanning electron microscopy; TCA, Trichloroacetic acid; TFA, Trifluoroacetic acid; WHO, World Health Organization's; WST-1, 2-(4-Iodophenyl)-3-(4-nitrophenyl)-5-(2,4-disulfophenyl)-2H-tetrazolium; WU, Water Uptake.

* Corresponding author. Department of Chemical Sciences and Technologies University of Rome Tor Vergata via della Ricerca Scientifica 00133, Rome, Italy.
E-mail address: sonia.melino@uniroma2.it (S. Melino).

[1] The authors equally contributed to the research.

https://doi.org/10.1016/j.biomaterials.2022.121984
Received 30 March 2022; Received in revised form 10 November 2022; Accepted 22 December 2022
Available online 23 December 2022
0142-9612/© 2022 The Authors. Published by Elsevier Ltd. This is an open access article under the CC BY-NC-ND license (http://creativecommons.org/licenses/by-nc-nd/4.0/).

Vegetables have been used as implantable and biocompatible cellulose scaffolds for 3D cultures of mammalian cells [14–16], and cellulose-porous based scaffolds have been also employed for osteoblastic differentiation of human mesenchymal stem cells and iPSCs (induced Pluripotent Stem Cells), exploiting the clinical prospective for their application as *in vivo* implants [17–19]. Human endothelial, pluripotent and mesenchymal stem cells have been implanted in both the inner surfaces of plant vasculature and in the outer surfaces of plant scaffolds preserving their functional properties [12].

Moreover, the great sustainability of the waste-vegetables and the need for producing new foods from vegetables with particular nutritional properties could be combined for the realization of new biomaterials for biomedical applications. Legumes, used in several diets including vegetarian, vegan, and mediterranean, are important ingredients in the lower-glycemic-index (GI) diets [20], in Dietary Approach to Stop Hypertension (DASH) eating plan, and are included in the World Health Organization's (WHO) Healthy Diet plan [21]. Legumes are a good source of bioactive compounds and phytochemicals including anthocyanins, phenolic acids, flavonols, and proanthocyanidins [22]. Particularly, the lupin shows several interesting health properties and recently it is becoming a major legume crop in Australia, especially in areas with potential environmental stress, annual rainfall <500 mm, and poor soil condition. Several studies suggest that the lupin consumption improves bowel function and reduces cholesterol, blood glucose, and glycemic index [23]. In the last years the *Lupinus* L. (family Fabaceae) has gained an increasing interest for its nutritional properties [24]. In ancient Greece and Egypt (earlier than 2000 BC), it was used as food for humans and feed for animals, and also in cosmetics and medicine. The medical and pharmaceutical value of lupin was known to Greeks as well as Romans. Seeds, plants and decoction left after seed soaking were employed as drugs. Plinius mentioned sixteen ways of applying lupin in medicine. Lupin hulls (LHs) contain 95% of fibers, mostly cellulose and hemicellulose, with large quantities of xylose and uronic acid, about 4–6% crude protein, lignin, carotenoids, tocopherols, polyphenols, minerals (ash) [25–30]and other bioactive components showing exciting potential [31]. Among them an interesting lipidic component is the lupeol [32] that is a triterpene alcohol belonging to a group of promising secondary plant metabolites. Lupeol has shown to improve the epidermal tissue reconstitution [33,34], to induce cellular differentiation and to inhibit the melanoma cells growth [35,36]. It is found in several other species and shows antinociceptive and anti-inflammatory properties [37–39]. Indeed, it seems to be a potent anti-inflammatory and multi-target drug, targeting key molecular pathways such as those involving NF-kB (nuclear factor kappa light chain enhancer of activated B cells), among others [40]. The treatment with lupeol induces a reduction of IL-4, IL-5 and IL-13 levels, that are characteristic of an allergic airway inflammatory process. Its anti-inflammatory feature is linked to its immune-modulatory and anti-tumor action [40–42]. Reduction of cellularity and eosinophils in the bronchoalveolar fluid in a murine model was observed after its administration [43].

In this work we have produced membrane scaffolds by the decellularization of Lupin hulls (LHs). LHs were characterized in terms of the microstructural features by scanning electron microscopy (SEM) and of the antimicrobial properties, and used as waste-vegetable biomaterial for the human cardiac Lin^- $Sca\text{-}1^+$ mesenchymal stem cells (hMSCs) growth. Moreover, a new bioplastic (BPLH) was here produced by an optimized LHs reprocessing protocol and characterized by microscopy, UV–vis fluorescence and FTIR spectroscopy, RP-HPLC and polyphenols analysis. The water uptake, degradability and antimicrobial properties of BPLH were also evaluated, as well as the mechanical properties. The scaffold capability of BPLH was assessed using both Normal Human Dermal Fibroblasts (NHDFs) and hMSCs, and a good cellular adhesion, proliferation and initial commitment toward muscle differentiation were observed over 2 weeks. This work represents a new approach toward the recovery and valorization of the vegetal waste for potential applications in biomedicine and for new formulation of stem cells based food.

2. Materials and methods

2.1. Scaffolds preparation

LHs were incubated for 24 h in ethanol under magnetic stirring at room temperature (23 °C) and after that, washed in H_2O_{dd} several times in order to completely remove the ethanol. Finally, they were lyophilized and stored in dried conditions at room temperature. The LHs were rehydrated with phosphate buffer solution (PBS) and cut in disks of 1 cm diameter.

BPLH scaffolds were produced incubating the dried and finely crushed LHs in anhydrous trifluoracetic acid (TFA) with a ratio of 0.3 g (d.w.)/ml for 48 h at 37 °C. The mixture was centrifuged for 30 min at 4000 rpm and the supernatant was put either in a petri dish or directly in the wells of a multiplate and immediately washed with PBS for several times, in order to normalize the pH.

2.2. Attenuated total reflection Fourier transform infrared spectroscopy (ATR-FTIR)

ATR-FTIR analysis of LH and BPLH was performed to characterize the functional groups present in the samples. It was carried out using a FTIR spectrometer (Jasco, FT/-6600) equipped with an attenuated total reflectance (ATR) cell. Spectra were recorded by placing and pressing the samples in contact with the ATR cell, in the following conditions: wavenumber ranged from 400 to 4000 cm^{-1}, spectral resolution of 2 cm^{-1} and number of scans 32.

2.3. Polyphenols extraction and total phenolic determination

Polyphenols were extracted with the following protocol: 33 mg LH and BPLH were incubated with 500 μl of 50% TCA (trichloroacetic acid) (w/v) overnight in ice. The samples were then centrifuged for 15 min at 10,000 rpm and the supernatant was recovered. Polyphenols quantification was performed using a modified Folin-Ciocalteu method [44]: 250 μl of Folin-Ciocalteu reagent (diluted 1:10 v/v) were added to 30 μl of TCA extracts for 4 min at room temperature in dark conditions. Then 20 μl of 1 M KOH and 200 μl of 1 M $NaHCO_3$ were added and the samples were incubated overnight in dark conditions. Finally, the absorbance at 750 nm was measured using an iMarkTM Microplate Reader (Bio-Rad). A calibration curve using gallic acid (0–20 μg) (see Fig. 1S) was performed in order to assess the polyphenols concentration, and the total phenolic content was expressed as gallic acid equivalents (GAE) (μg/mg of dry weight).

RP-HPLC analysis of the TCA extracts was performed using mod. LC-10AVP (Shimadzu, Milan, Italy), equipped with a UV detector (Shimadzu, Milan, Italy) and a C18 column (150 mm × 4.6 mm, 5 μm, CPS Analitica, Rome, Italy), loop of 20 μl, rate flow 0.8 ml/min. The solvent B gradient (solvent B: 80% CH_3CN, 0.1% TFA; solvent A: 0.1% TFA) used was: 0–5 min 0%; 5–65 min 60%; 65–90 min 90%. The elution was monitored at 220 and 280 nm.

2.4. Water uptake of BPLH

Water uptake study was performed to determine the water holding capacity of BPLH. Briefly, BPLH disks (1 cm of diameter) were immersed in distilled water at room temperature (25 °C) and, at different times (0, 3, 5 and 24 h), the samples were removed from water and weighed. The water uptake of the matrices was calculated by the following equation (eq. 1) [13,45]:

$$\text{Water Uptake } \% = \frac{W_{wet} - W_{dry}}{W_{wet} + W_{dry}} \times 100 \qquad \text{eq.1}$$

where W_{wet} and W_{dry} are the weights of the wet and dried BPLH, respectively.

2.5. Degradability

The degradability of the starch-based bioplastic disks (1 cm diameter) was determined by dipping them in different solutions (1 ml) (i.e. H_2O_{dd}, 1 M NaOH, 1 M HCl and 1:10 E:S (w/w) trypsin solution in 10 mM Hepes buffer pH 8.5), incubated at 37 °C and monitored over 6 weeks.

2.6. Analysis of the mechanical properties

Mechanical properties of BPLH were investigated by uniaxial tensile tests performed on dog-bone specimens (width 4.8 mm, length 22.00 mm), at 5 mm/min to rupture by an electromechanical machine (Lloyd LRX), equipped with a 500 N load cell, at 25 °C, following ASTM D882 standard. Four specimens were prepared and all mechanical properties were calculated considering the nominal specimen cross-section.

2.7. Analysis of the antimicrobial property

The antimicrobial activity of both LH and BPLH was tested using ampicillin resistant *E.coli* (*E.coli*^{AmpR}) BL21 strain grown either in solution with LB medium or onto petri dishes with agar-LB medium, both with 100 μg/ml of ampicillin. The disks (diameter 1 cm) were previously sterilized using ethanol and UV exposure and after the solvent evaporation, they were placed either in the LB medium or on the petri dishes in case of BPLH both seeded with the bacterial overnight culture and incubated at 37 °C. The cultures in LB solution were followed on time for about 5 h detecting the optical density at 600 nm, while the cultures in petri dishes with LB agar were incubated overnight and the inhibition of the bacterial growth around the disks was analyzed.

2.8. Cellular cultures

Sca-1$^+$ Lin$^-$ human cardiac mesenchymal stem cells (hMSCs) line was previously obtained by Forte G et al. [46] using cell sorting from auricular biopsies made during coronary artery bypass surgery. Both hMSCs and normal human dermal fibroblasts (NHDFs) (Lonza, Basel, Switzerland) cell lines were cultured in Dulbecco's Modified Eagle Medium (DMEM) (Gibco, Italy), containing 10% Fetal Bovine Serum (FBS) (Gibco, Italy), 1% penicillin-streptomycin (Sigma-Aldrich, Italy), 1% L-Glutamine (Gibco, Italy), herein referred as to "complete medium". LH scaffolds were washed with PBS for 2 days and conditioned for 3 days with complete medium before cell seeding.

2.9. Cell adhesion and viability assays

The cell adhesion and proliferation of the hMSCs and NHDFs on LH or BPLH were evaluated by MTT and/or WST-1 assays. The cellular adhesion was evaluated using the following protocol: the cells were seeded at a cellular density of 5×10^3 cells/cm^2 and after 5 h from seeding, the LH or BPLH scaffolds were transferred into new wells, and the samples were incubated for 3 h in DMEM medium high glucose without phenol-red at 37 °C with 5% CO_2 in the presence of 10% v/v of 5 mg/ml 3-(4,5-dimethyl-2-thiazolyl)-2,5-diphenyl-2H-tetrazolium bromide (MTT) solution in PBS buffer, [47]. Subsequently, the medium was discarded and the precipitated formazan salts were dissolved into 500 μl of DMSO/acid isopropanol mixture applying 18 kHz ultrasounds for about 1min at the air-water interface by means of a Sonics and Materials ultrasound generator (Branson) with a 3 mm in diameter horn at an applied acoustic power of 160 Wcm^{-2}. The optical density of the solution was evaluated using a spectrophotometer at a wavelength of 570 nm. The cell viability of both hMSCs and NHDFs on BPLH was obtained using Water-Soluble Tetrazolium salt (WST-1) assay (2-(4-Iodophenyl)-3-(4-nitrophenyl)- 5-(2,4-disulfophenyl)-2H-tetrazolium) (Roche Diagnostics, Sigma Aldrich, Italy) [48]. Briefly, the samples were incubated for 3 h in DMEM medium high glucose without phenol-red in the presence of 5% (v/v) cell proliferation reagent WST-1 at 37 °C with 5% CO_2. The absorbance of the medium was evaluated using an iMarkTM Microplate Reader (Bio-Rad) at a 450 nm wavelength.

2.10. Fluorescence and immunofluorescence analyses

hMSCs were seeded on LH and BPLH scaffolds at cellular density of 2×10^4 and 3×10^4 cells/cm^2, respectively and cultured with complete medium for 1, 2 and 3 weeks. After washing with PBS, the samples were fixed in 4% paraformaldehyde (PFA) in PBS for 15 min at 4 °C, permeabilized with 0.2% v/v Triton X-100 (Sigma-Aldrich, Italy) for 15 min and incubated with antibodies specific for α-smooth muscle actin (α-SMA) and α-actinin (Sigma-Aldrich, Italy), followed by the appropriate Alexa fluorochrome-conjugated secondary antibodies (Invitrogen, Italy). Nuclei were stained with Hoechst 33342 (Sigma-Aldrich, Italy). The cell growth on BPLH of both NHDFs and hMSCs was analyzed by fluorescence microscopy fixing and staining the cells with a crystal violet solution (6% v/v glutaraldehyde and 0.5% w/v crystal violet in deionized water) and then washing with PBS. Epifluorescence microscopy was performed using the Zeiss fluorescence microscope Axioobserver 7 Zeiss, while the confocal micrographs were obtained using both a confocal laser scanning microscopy Olympus Fluoview 1000 and a Stellaris Leica microscope platform for the hMSCs and the NHDFs samples on BPLH, respectively.

2.11. Microstructural characterization by HR-SEM analysis

The scanning electron microscopy micrographs of the LH samples with and without hMSCs and BPLH were acquired with a Zeiss Leo Supra 35 field emission gun scanning electron microscope (FEG-SEM, Cambridge Leo Supra 35, Carl Zeiss). The samples of LH with hMSCs were prepared using increasing percentages of ethanol in agreement with previous described protocols [14], then the samples were frozen in liquid nitrogen and fractures of the samples were performed. The fragments of the freeze-dried BPLH, lupin hulls and the lupin hulls with hMSCs were placed on carbon tape and metalized under vacuum before SEM analysis.

2.12. Statistical analysis

GraphPad Prism version 6.0 (GraphPad Software, San Diego, CA, USA) was used for the statistical analysis. Data obtained from three or five independent experiments were analyzed for each variable using ANOVA One-way test or a one-tailed Student's t-test. A p-value <0.05 was considered to be statistically significant.

3. Results

3.1. Preparation and characterization of decellularized LH scaffolds

Dried LH scaffolds were prepared as described above and then were hydrated using PBS and cut in disks of 1 cm diameter. An ultrastructural analysis by SEM was performed. In Fig. 1 the micrographs of the inner and outer side of the LH scaffold are shown. While the inner side is smooth (Fig. 1A), the outer side of LH is characterized by the presence of physiological micro-porosity (Fig. 1B), with pores of about 10 μm; this system of membranes could have a physiological relevance in the *gas* permeability, conferring a property that should be investigated.

The antimicrobial activity of LH scaffold and fresh lupin hulls (FLHs) was evaluated using BL21 *E. coli* strain ampicillin resistant. The growth of *E.coli*^{AmpR} was significantly reduced in the sterilized LB medium, where one LH disk was incubated at 4 °C for 4 days. In Fig. 1D the

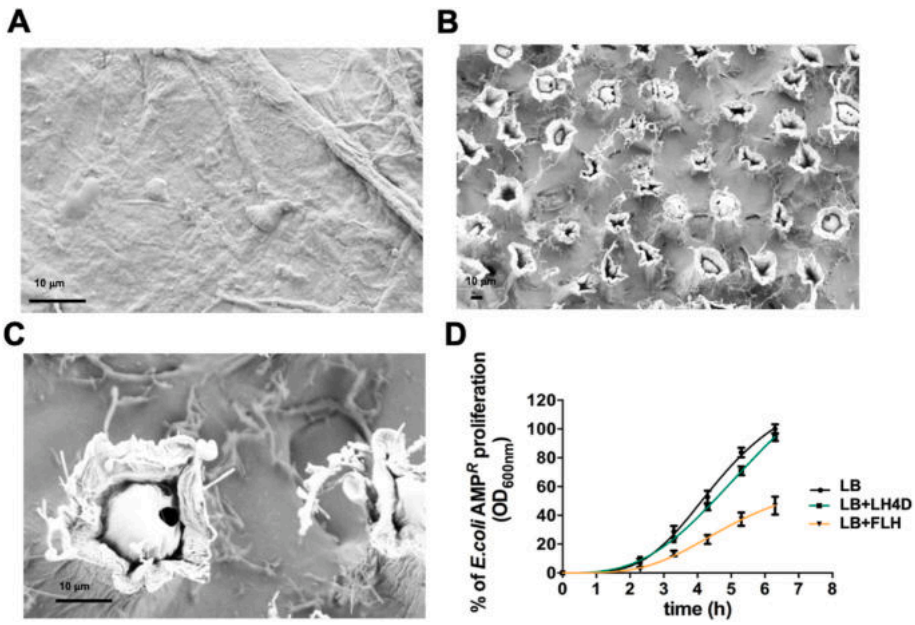

Fig. 1. Microstructural characterization of LH and antimicrobial property of LH and FLH. (A) SEM micrograph of the LH inner surface (magnification 5kx). SEM micrographs of the LH outer surface (magnification:1kx in (B) and 5kx in (C)) with pores of about 10 μm. Scale bars are of 10 μm. (D) *E. coli* ^{AmpR} growth is obtained by $OD_{600\ nm}$ over the time. The *E.coli* growth was performed in LB medium with 100 μg/ml ampicillin (black line) and in the presence of LH (green line) or FLH (orange line). LH was previously incubated in LB for 4 days in sterile conditions and then the LB was used for the *E. coli* growth. Experiments were performed as three biological replicas. Error bar indicates S.D. (For interpretation of the references to color in this figure legend, the reader is referred to the Web version of this article.)

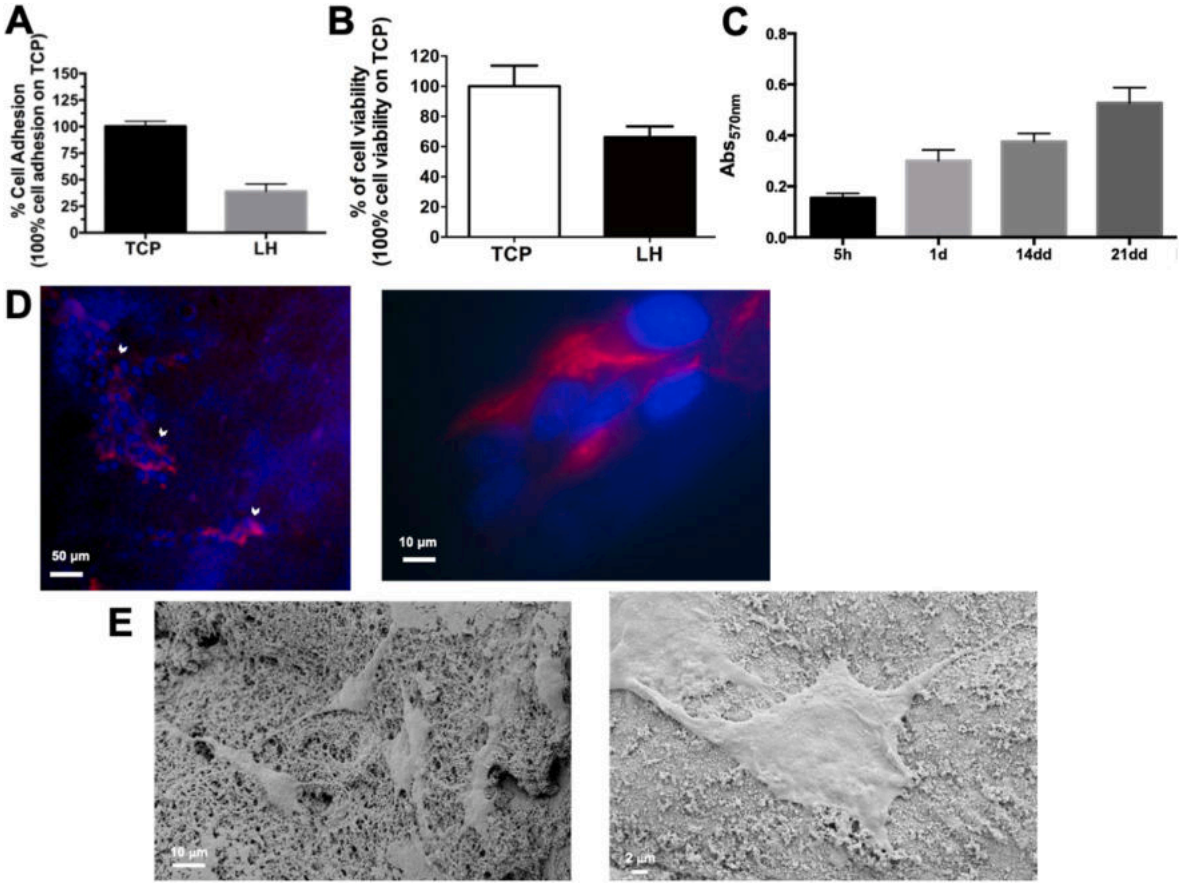

Fig. 2. Stem cell adhesion and proliferation on LH scaffold. (A) hMSCs (seeded at 5×10^3 cells/cm^2) adhesion to the LH scaffold after 5 h from seeding. Cell proliferation of hMSCs after (B) 7 days and (C) over time at 5 h, 1, 14 and 21 days of growth. Experiments were performed as three biological replicas. Error bar indicates S.D. (D) Fluorescence micrographs of hMSCs on LH scaffold after 7 days of growth. Nuclei are stained with Hoechst 33,342 and the α-SMA protein is in red. The arrows indicate the presence of α-SMA protein. Scale bars are of 50 μm and 10 μm. (E) SEM micrographs of hMSCs on LH scaffold after 21 days (Mag. 2kX and 3kX and scales bars of 10 μm and 2 μm). The arrows indicate the presence of α-SMA protein. (For interpretation of the references to color in this figure legend, the reader is referred to the Web version of this article.)

profiles of the bacterial growths using LB medium conditioned or not with LH/FLH disks are shown. A high reduction of the bacterial growth was observed in the case of FLH, but also the LH presence induced a slowdown in growth. This antimicrobial activity can be attributed to a release of antibacterial phytochemicals from LH/FLH. In order to identify the substance present on the LH an extract with 50% of TCA was performed and analyzed by RP-HPLC.

3.2. Efficiency of hMSCs adhesion and proliferation on LH

The outer surface of LH is characterized by the presence of pores but also of waxes, which represent a physiologically important barrier to microbes and external substances and minimize the water loss. The presence of the waxes reduced also the cellular adhesion and proliferation as observed by preliminary experiments (data not shown), therefore we performed the cell seeding on the inner surface. In order to use the LH as scaffold for cell cultures, the cell adhesion of hMSCs on LH scaffold of 1 cm diameter was evaluated. hMSCs (5×10^3 cells/cm^2) were seeded on the inner surface of the LH scaffold and both cell adhesion after 5 h and proliferation over the time were assessed by MTT cell viability assay. The cell viability (after a total of 5 h from seeding) of a control consisting of hMSCs on TCP (Tissue Culture Plate) and of hMSCs that had adhered to the LH scaffold was then compared. In Fig. 2 the metabolic analyses of the hMSCs cultures grown on LH scaffold are shown. The hMSCs adhesion on LH scaffold was 34.2% ± 6.8 SD compared to the cell adhesion on TCP (100%) (Fig. 2A), suggesting a good adhesion efficiency of the hMSCs on LH scaffold. The hMSCs proliferation on LH scaffold after 7 days (Fig. 2B) and over time until 21 days was also analyzed (Fig. 2C), demonstrating that the vegetal LH scaffold can be a good material for supporting the cell growth.

The immunofluorescence microscopy analysis of the samples is shown in Fig. 2D. It was obtained using Hoechst *in vivo* staining of the nuclei and the alpha-smooth muscle actin (α-SMA) antibody. This preliminary analysis shows the absence of pyknotic nuclei and a good expression of the α-SMA after 7 days, poorly expressed originally in hMSCs, indicating an initial commitment of the stem cells differentiation process. SEM micrographs of the samples after 21 days of growth are shown in Fig. 2E, and allow to visualize the interaction of the cells with the scaffold. In particular, it is possible to see an elongated morphology of the hMSCs on LH scaffold, being an index of efficient adhesion to the scaffold, and cellular connections, indicating a good cell-cell interaction.

3.3. BPLH production process and microscopic and spectroscopic characterization

The high content of structural polysaccharides, such as cellulose, hemicellulose and pectins [23], in the lupin peel suggested the possibility of making a bioplastic from LH. The protocol used by Bayer et al. [49] was optimized for creating a homogeneous and flexible bioplastic in less time, after incubation of the TFA mixture for 48 h at 37 °C and subsequent centrifugation at 10,000 rpm for 30 min (Fig. 3A). The bioplastic from LH was named BPLH and its digital images and optical micrographs are shown in Fig. 3B and C. It is possible to observe a highly uniform surface by optical microscopy, without evident presence of particulates. The surface morphology of BPLH was assessed by SEM analysis. In Fig. 3D are shown the micrographs performed at 10 kx and 20 kx of magnification that confirm a flat surface of the biomaterial with nano-roughness.

In Fig. 4A the BPLH absorption spectrum is shown. A maximum around 500 and 400 nm is visible, in accordance with the BPLH reddish color. Fluorescence analysis was also observed by exciting the sample at 408 nm (Fig. 4B), with emission at 450 nm in the violet/blue range.

FTIR analysis was also carried out for both LH and BPLH in order to obtain comparative information and to check any difference (Fig. 4C). BPLH shows the typical FTIR profile of cellulose with the characteristic peaks related to the stretching of the C–O group at 1020 cm^{-1} and the glycosidic-C1H deformation at 897 cm^{-1} as reported by Raspolli et al. [50]. The large and intense band at 3355 cm^{-1} is instead attributable to

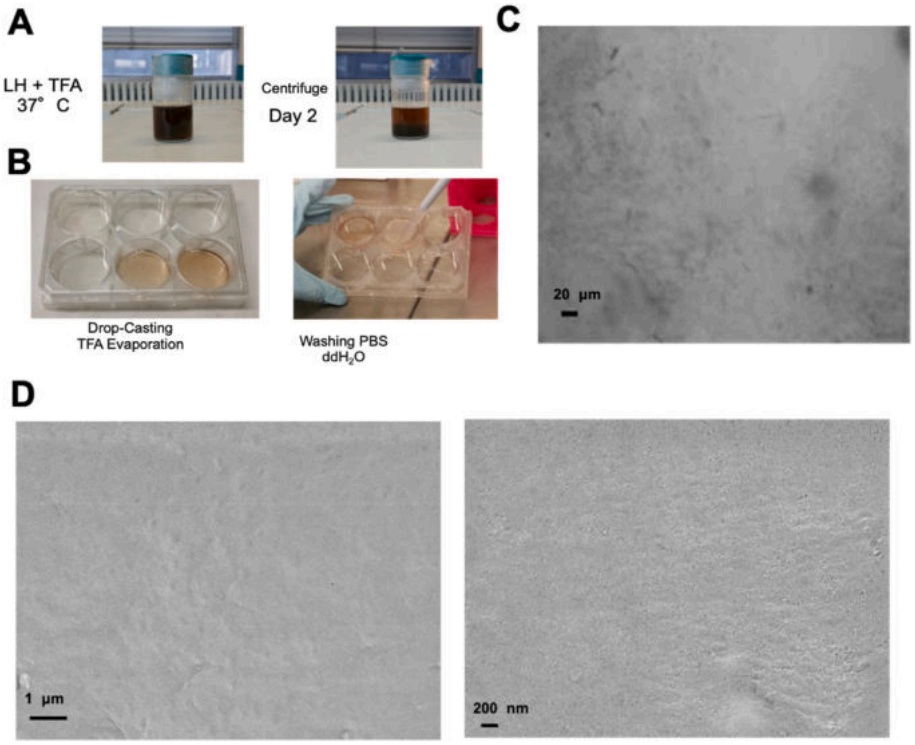

Fig. 3. Production and morphological characterization of BPLH. (A) BPLH schematic production process and digital photographs of BPLH. LHs were incubated with anhydrous TFA, then centrifuged and dropped. After TFA evaporation, the bioplastic was washed with PBS (B); (C) Bright-field micrographs of BPLH scale bar of 20 µm; (D) SEM micrographs at Mag. 10 kx (1 µm) and 20 kx (200 nm).

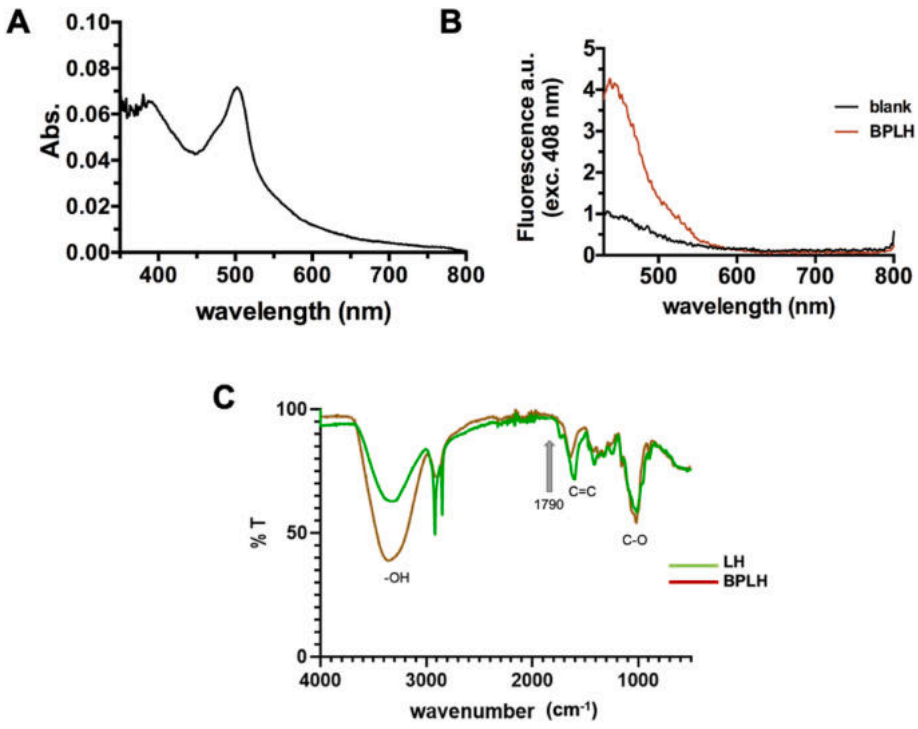

Fig. 4. BPLH physical-chemical characterization by UV–Vis and FTIR spectroscopy. (A) Absorption spectrum of BPLH (wavelength range of 400–800 nm) and (B) fluorescence spectrum (emission wavelength range of 400–800 nm; excitation wavelength of 408 nm). (C) FTIR spectra of LH (green line) and of BPLH (dark red line) performed with the following parameters: wavenumber range of 400–4000 cm^{-1}, spectral resolution of 2 cm^{-1}, 32 scans. (For interpretation of the references to color in this figure legend, the reader is referred to the Web version of this article.)

the vibration of the –OH groups, suggesting the presence of strong intermolecular hydrogen bonds between cellulose macromolecules. Finally, it is possible to note the peak at 2904 cm^{-1}, characteristic of the elongation vibration of the alkyl groups. From the FTIR analysis, Ritcey AM et al. [51] showed how the dried films are trifluoroacetylated after their formation and TFA evaporation, with the presence of a significant peak at 1790 cm^{-1} in the spectrum.

However, this esterification was found to be only temporary, as it was spontaneously removed in the presence of water or in a humid atmosphere (60% RH) after 1–2 days. In fact, from the observation of the FTIR spectrum of the BPLH, after TFA evaporation and washing with PBS, the presence of this peak was not found, suggesting the complete elimination of acid traces.

Although from the comparison of the LH and BPLH spectra common characteristic peaks are visible (Table 1), particularly in the fingerprint area, it is possible to see some differences, namely the disappearance of two peaks following the reaction with TFA: the first at 2854 cm^{-1} related to the symmetrical stretching of the methylene group and the second at 1733 cm^{-1} associated with the stretching of the carbonyl group.

3.4. Polyphenols in LH and BPLH scaffolds

With the aim to analyze and compare the presence of phytochemicals with antioxidant properties in both LH and BPLH, the polyphenols content was determined. An extraction of the phytochemicals was performed by incubation of 33 mg of dried sample in 1 ml of 50% TCA overnight in ice and dark conditions. The two supernatants were analyzed by RP-HPLC either at 220 or 280 nm and the chromatographic profiles are shown in Fig. 5A and B. Some little differences are visible between the two extracts, in agreement with the results obtained by FTIR analysis, demonstrating that the phytochemicals are conserved in the BPLH after the LH reprocessing.

Table 1
Functional groups of LH and BPLH identified by ATR-FTIR analysis.

Functional groups	LH BPLH wavenumber (cm^{-1})	
O–H	3330	3346
C–H	2918	2904
C=C	1612	1619
C–O	1020	1021
Glicosidic group	893	897

Moreover, the total polyphenol determination by Folin-Ciocalteu assay showed the presence of 2.18 μg (GAE)/mg (d.w.) and 0.64 μg (GAE)/mg (d.w.) of polyphenols for BPLH and LH, respectively (Fig. 5C). This result linked to a higher availability and easier release of the polyphenols in the case of the bioplastic could be due to the used degradation protocol.

The antimicrobial activity of BPLH was also tested using the ampicillin-resistant strain of BL21 *E. coli*^{AmpR} grown on LB agar medium (as shown in Fig. 2S), but the BPLH in the considered conditions did not show any antimicrobial activity, probably due to a low antimicrobial compounds release.

3.5. BPLH water-uptake and degradability

The degradability of BPLH was tested incubating the BPLH in H_2O_{dd}, 1 M HCl, 1 M NaOH or 1:10 E:S (w/w) trypsin solution in 10 mM Hepes buffer, pH 8.5, for 6 weeks. In Fig. 6Ab), no fractures or initial sample degradation appeared when the BPLH was incubated in H_2O or HCl and trypsin solution (data not shown), but the degradation process was accelerated in basic conditions, using 1 M NaOH solution, with a significant degradation of the BPLH (Fig. 6Ac). Water uptake tests were performed to evaluate the hydration capacity of the bioplastic and to have a qualitative measure of its hydrophilicity degree. The percentage of water uptake (% WU) by the bioplastic was evaluated at time intervals up to 24 h. The test results (Fig. 6B) show how the sample, immersed in double distilled water at 37 °C, reaches a plateau of 400% WU after just a few minutes, keeping it almost constant for the rest of the investigated interval time. The bioplastic obtained is characterized by a high hydration rate. Interestingly, after two months from the sample preparation, the test was repeated, confirming the hydration rapidity, but with a maximum value of about 300% WU (Fig. 6B). This reduction in the initial hydration capability can be due to the aging of the sample,

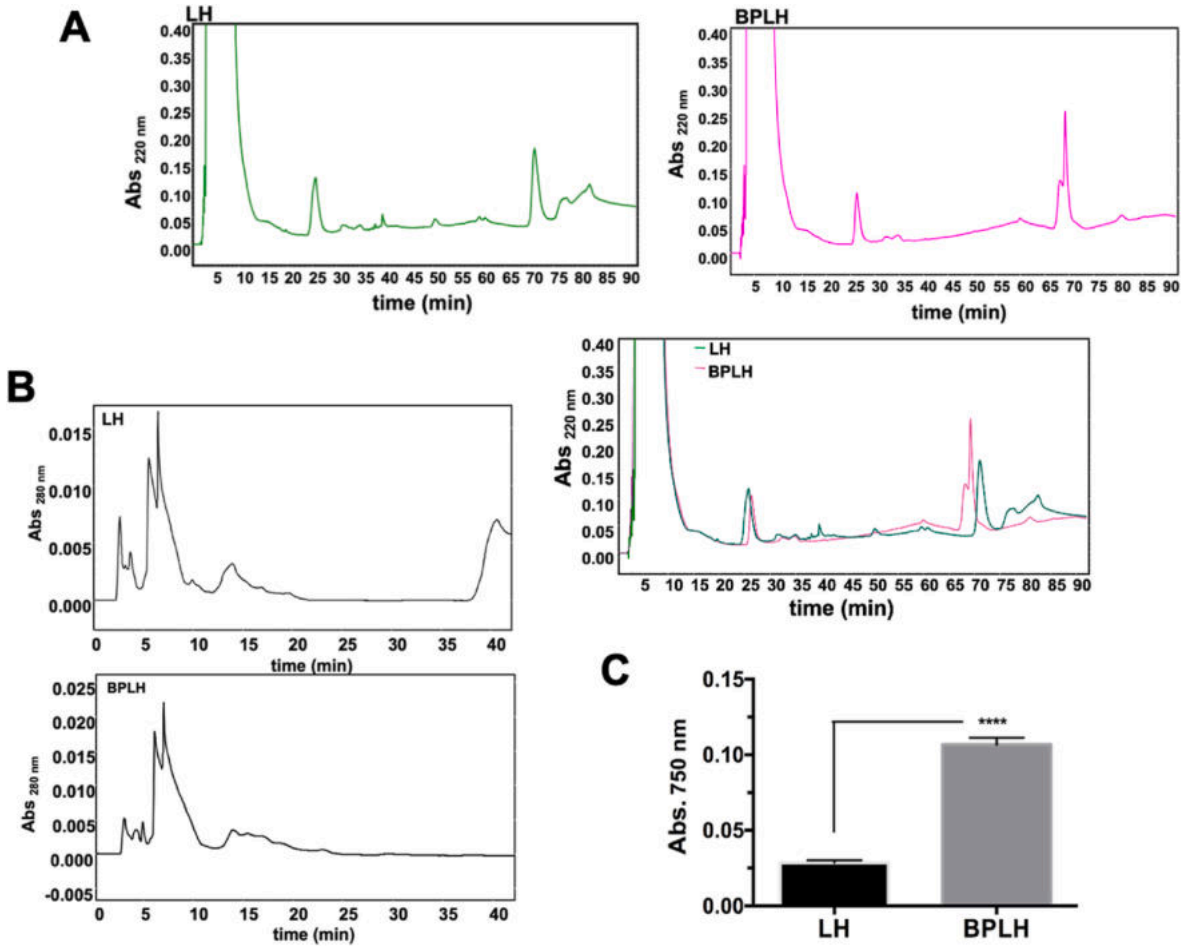

Fig. 5. Determination of polyphenols content in LH and BPLH. (A) RP-HPLC chromatograms of the BPLH and LH extracts in TCA obtained with the following parameters: solvent B gradient: 0–5 min 0%; 5–65 min 60%; 65–90 min 90%. The absorbance at 220 nm (A) and 280 nm (B) was monitored. (C) LH and BPLH polyphenols content obtained by Folin-Ciocalteu assay, measuring the absorbance at 750 nm. The results were obtained by five or six independent measurements. Error bar indicates S.D. ****p value $\leq$ 0.0001.

suggesting that the WU could be used as a parameter in order to assess the bioplastic aging.

3.6. Mechanical properties of BPLH

The mechanical properties of the bioplastic obtained from the lupin peel were analyzed through tensile tests in order to determine the elastic modulus and the breaking load. The modulus was determined as the slope of the linear section of the stress/strain curve at low strains, while the breaking load was corresponding to the value recorded at failure, considering that the material has showed an elastic-brittle behavior. The typical stress-strain curve obtained is shown in Fig. 6C.

The final mean value of the elastic modulus was 0.08 ± 0.02 MPa, while that of the breaking load was 3.5 ± 0.9 MPa. In Table 2 the calculated Young modulus and the breaking load for the 4 specimens are reported.

3.7. BPLH as scaffold for cell growth of NHDFs and hMSCs

BPLH was tested as scaffold and the cell adhesion and proliferation were assessed using both NHDFs and hMSCs in order to compare the behavior of different cell types. In particular, NHDFs were seeded on BPLH scaffold (2 cm^2 of growth area) and the cell proliferation was assessed after 10 and 21 days (see Fig. 7A). With the aim to evaluate the viability of the cells really adhered to the scaffold, after 24 h and before the WST-1 assay, each BPLH scaffold with NHDFs was transferred into a new well. A gradual increase in the cell growth of the NHDFs adhered to the scaffold was observed. Fig. 7B shows the confocal micrographs of the NHDFs seeded at a cell density of 2×10^4 cells/cm^2 on BPLH after 3 days of cell growth. Optical and fluorescence microscopic analyses were performed staining the cells with crystal violet. The quality of the images obtained using the optical microscopy was not good (see Supplementary Materials Fig. 3S), probably due to the optical interference of the bioplastic. Therefore, samples were analyzed by fluorescence microscopy, taking into consideration the fluorescence property of the crystal violet.

A spindle morphology of the cells is observable indicating a good adhesion of the fibroblasts to the BPLH. Moreover, the expression of the α-SMA protein was detected after one week of cell growth onto the BPLH, indicating the possible *trans*-differentiation of the fibroblasts into myofibroblasts (Fig. 7C and D), that was not expressed after 1 week of cell growth on TCP (see Fig. 4SA). NHDFs seeded on TCP and grown in presence of BPLH for 12 days were also analyzed by fluorescence microscopy (see Fig. 4SB) and only a change in the nuclei size was observed, probably due to the phytochemicals release. Therefore, it was demonstrated that only the cell growth on BPLH was capable to promote the expression of α-SMA at short times. These results demonstrated that BPLH could represent a good scaffold for dermal cells growth and repair.

The cell viability after 3 and 7 days of hMSCs was also assessed by MTT metabolic assay (Fig. 8A). The active hMSCs metabolism after 3 days, with a 40.5% (SD ± 6.6) of cell viability respect to the control (cells grown on TCP), suggests a good adhesion efficiency and growth of the hMSCs on the BPLH scaffold, and a good percentage of cell

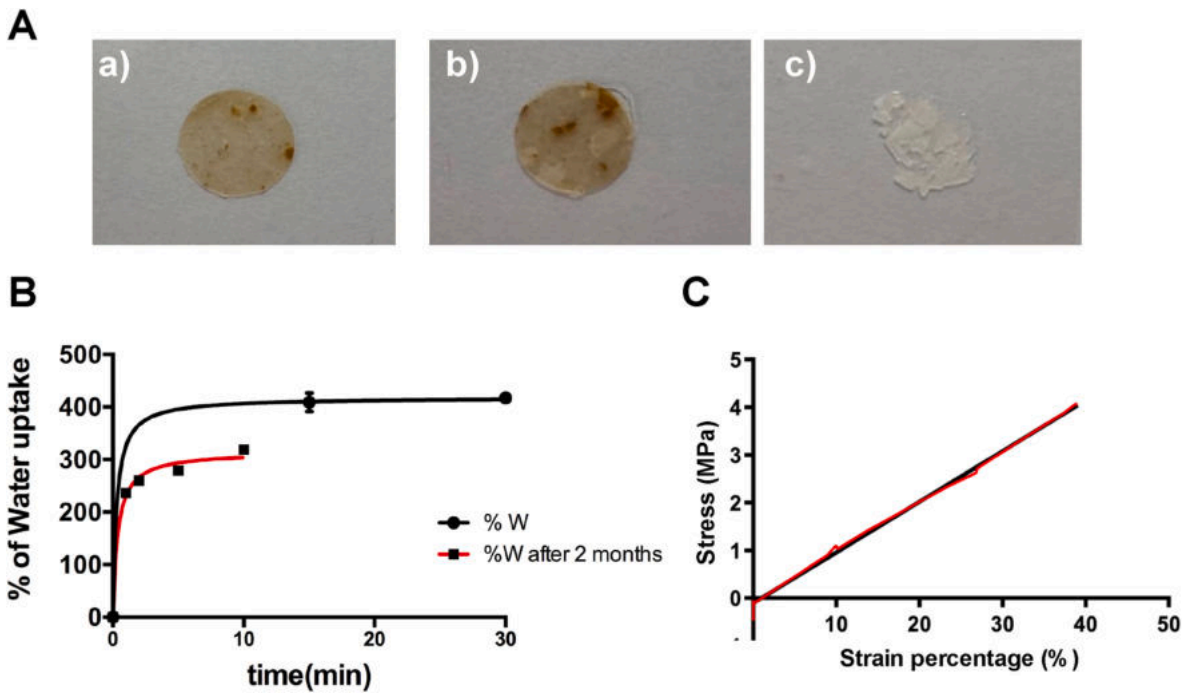

Fig. 6. Degradability and water-uptake and mechanical properties of BPLH. (A) Digital photographs of BPLH disks (diameter 1 cm) at day 0 (a)) and after 6 weeks at 37 °C in H_2O (b)) and in NaOH 1 M (c)). Three replicas of each sample have been performed. (B) Water absorption percentage of BPLH soon after its production (black line) and after 2 months (red line). The data were obtained by three independent experiments. Error bar indicates S.D. (C) Representative stress-strain curve obtained using a preload of 500 N, rate of 5 mm/min, length of 22 mm, width 4.8 mm, temperature of 25 °C. (For interpretation of the references to color in this figure legend, the reader is referred to the Web version of this article.)

Table 2
Mechanical properties of BPLH. Calculated Young modulus and breaking load (MPa) for each of the 4 specimens. The r^2 value for each stress-strain curve is reported.

Samples	Young modulus (MPa)	Breaking load (MPa)	r^2
1	0.08727	3.1534	0.9956
2	0.1061	4.518	0.9969
3	0.05525	2.504	0.9955
4	0.07723	3.8643	0.9984

proliferation after 7 days was also found.

The fluorescence microscopy (see Fig. 8B), also in this case, revealed the presence of a high number of cells that were well attached to the biomaterial with an elongated morphology and cellular interconnections. Hoechst 33,342 staining *in vivo* after 2 weeks of growth was also carried out suggesting a good cell viability of hMSCs on the BPLH scaffold (see Fig. 8C). Moreover, confocal microscopy was performed using the crystal violet staining, observing a good potential use of this staining for this type of samples (Fig. 8D and E, video 1S). It was very complex to perform a confocal microscopy analysis for these samples using fluorochromes such us Hoechst and Alexa fluorochrome-antibodies, probably due to the optical and intrinsic fluorescence properties of the BPLH scaffold.

Supplementary video related to this article can be found at https://doi.org/10.1016/j.biomaterials.2022.121984

3.8. hMSCs growth and differentiation on BPLH scaffold

hMSCs were able to grow on the BPLH scaffolds for several weeks and a high cell viability even after 3 weeks was detected (Fig. 9A). The expression of some proteins and the status of the nuclei of the hMSCs grown on BPLH scaffold were evaluated by immunofluorescence microscopy after 3 weeks of growth, using Hoechst *in vivo* staining and anti- α-actinin and anti- α-SMA Alexa fluorochrome-antibodies (Fig. 9B, C and 9D). The cells were organized in bundles and interacting with each other; the presence of intact cell nuclei was observed, while it was not possible to acquire confocal microscope images due to the interference of the biomaterial in the analysis and it was not possible to evaluate the expression of the two proteins by fluorescence microscopy.

The great handiness of BPLH with attached cells (see video 2S) may suggest the possibility to use this cell-functionalized material for biomedical applications in wound healing and for the creation of new food combining the animal and vegetable kingdoms.

4. Discussion

Recently, the potential market for the application of lupin has widened thanks to the properties of its proteins including: non-animal dairy products, meat analogues, baby food formulations etc. [31, 52–54]. Therefore, the recovery and valorization of this leguminous waste could represent a possibility for the development of associated reprocessing-waste industry. Here, vegetable scaffolds by lupin hulls have been created and characterized in order to recover and enhance a vegetable waste for potential applications in stem cell growth. Firstly, a protocol was developed to use the lupin hulls for the production of LH membrane scaffolds and an ultrastructural characterization by SEM and evaluation of the antimicrobial property were carried out. The observed natural micro-porosity suggested a potential semi-permeability of the LH scaffold that could also allow *gas* exchanges. Moreover, although the preparation process for the LH led to a decrease respect to the fresh lupin peel, the antimicrobial activity was conserved, demonstrating the potential release of the antibacterial phytochemicals. Our *in vitro* studies demonstrated the LH scaffold biocompatibility and its potential use as scaffold for stem cell growth. It was demonstrated that LH is capable to promote the cell adhesion and the formation of cell connections, as well as the cell proliferation, in the case of human cardiac MSCs. Immunofluorescence analyses revealed the presence of a high percentage of

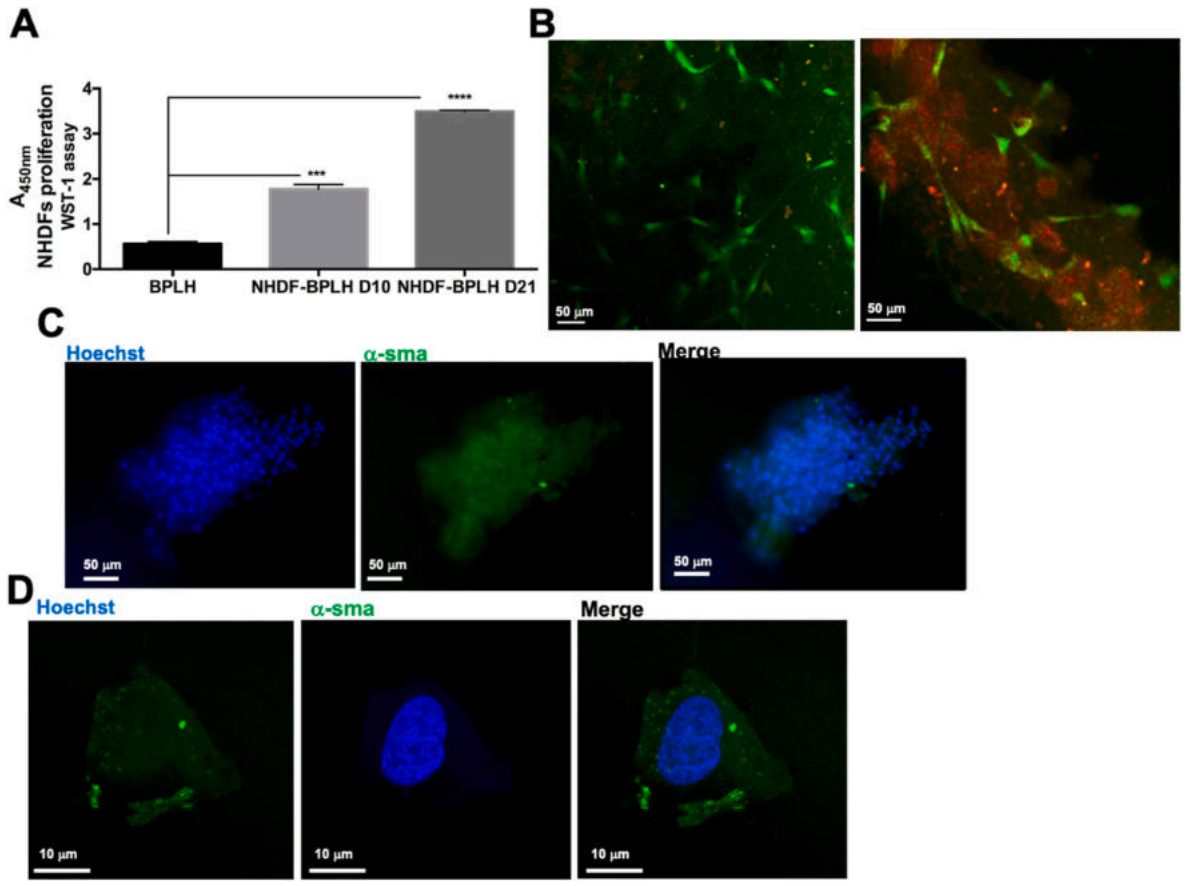

Fig. 7. BPLH as scaffold for NHDF lines. (A) Cell proliferation of NHDFs (seeded at 10^4 cells/cm^2) on BPLH scaffold measured after 10 and 21 days of growth. (B) Confocal fluorescence micrographs of NHDFs seeded at a cellular density of 2×10^4 cells/cm^2 on BPLH scaffold after 3 days of cell growth and stained with crystal violet, by excitation at the wavelengths of 495 nm and 568 nm; (C) fluorescence micrographs of NHDFs growth for 7 days on BPLH scaffold, the nuclei are stained with Hoeschst 33,342 (in blue) and the expression of α-SMA protein is detected in green. (D) Confocal fluorescence micrographs of NHDFs after 1 weeks of growth on BPLH obtained by the overlapping of 44 slices. The nuclei are stained with Hoeschst 33,342 (in blue) and the expression of α-SMA protein is detected (in green). Scale bars are of 50 μm and 10 μm for Mag. 20X and 40X respectively. ***p value $\leq$ 0.001 and ****p value $\leq$ 0.0001. (For interpretation of the references to color in this figure legend, the reader is referred to the Web version of this article.)

intact cell nuclei and the increased expression of the α-SMA protein, suggesting the ability of the scaffold to induce an initial commitment of the hMSCs differentiation process. Future studies on gene expression will allow us to verify the expression of α-SMA and other proteins involved in the muscle-differentiation process. In recent years, several plant-based scaffolds have been employed for *in vitro* 3D culture for tissue engineering [13,55–57]. Decellularized apple scaffold was used for MC3T3-E1 pre-osteoblasts demonstrating their good adhesion, proliferation and osteoblastic differentiation [19]. In a previous work, we demonstrated the scaffolding properties of micro-structured 3D scaffolds derived from broccoli waste [13]. Therefore, the here demonstrated LH capability to support the human stem cells survival, proliferation and cell-cell interaction indicates the feasibility to use a natural material from waste with antimicrobial property as stem cell-scaffold system.

Stalks of parsley and spinach, together with cocoa and rice husk, have been previously employed for the production of cellulose-based bioplastics through the use of trifluoroacetic acid [49]. Therefore, here a new bioplastic from LH was also produced using an optimized protocol previously described by Bayer et al. [49]. BPLH properties were investigated in order to obtain a complete characterization of the new biomaterial. The analysis of the BPLH and LH molecular spectra, obtained by FTIR spectroscopic characterization, showed for both samples the typical cellulose profile, in agreement with the chemical composition of the used vegetable waste. Furthermore, the absence of the characteristic peak of trifluoroacetylated cellulose in the bioplastic spectrum has allowed us to deduce the elimination of any acid trace by washing with PBS.

The data obtained by water uptake and degradation tests show the ability of BPLH to rapidly absorb a considerable amount of water and have a greater stability over time compared to other vegetable bioplastics [58]. The results also highlighted a fragmentation of the bioplastic in an alkaline environment, demonstrating that the basic hydrolysis, in contrast to acid and enzymatic hydrolysis, is able to promote an acceleration of the BPLH degradation process. BPLH results more resistant than other bioplastics from vegetables that were completely degraded after one month [49] or than the thin film of nanocellulose produced by skin of the jackfruit (*Artocarpus heterophyllus*) that was rapidly degraded by acid hydrolysis [58]. Moreover, the water uptake of BPLH was 4 folds greater and rapid than the other bioplastics [58]. An elastic-brittle behavior of the bioplastic, in terms of Young modulus and breaking load, was observed. Our results combined with other previous studies using vegetable-waste derived material suggest the possibility to design and manufacture biomaterials with customized mechanical properties that can respond to specific application needs, ranging in different areas, from packaging to biomedicine [59–62]. Varying the vegetable species, it is possible to obtain materials carrying different biochemical, physical and mechanical properties.

Moreover, the determination of the total polyphenols content in both LH and BPLH was performed demonstrating that the reprocessing process used for the BPLH production doesn't induce the degradation of the phytochemicals, such as the polyphenols, that can confer to the bioplastic antioxidant properties. This represents an important natural

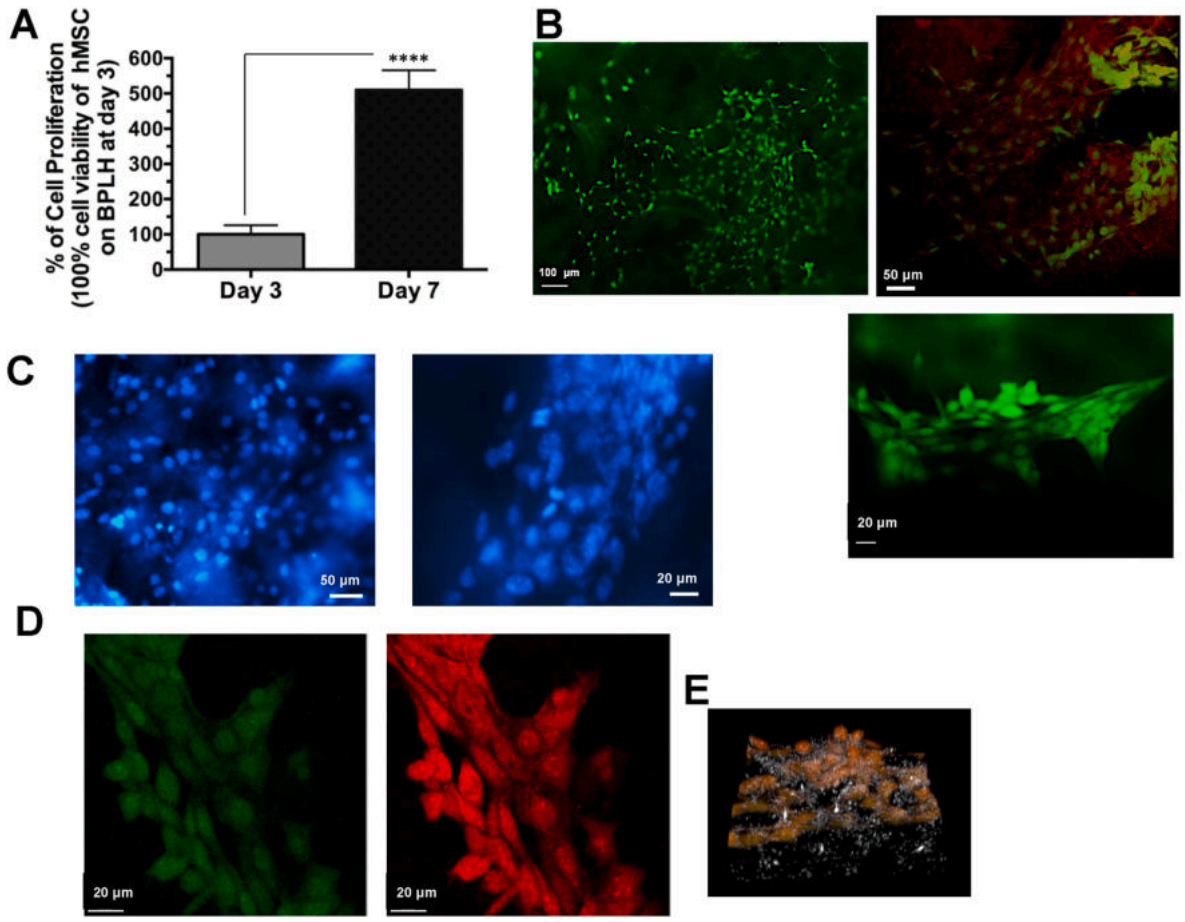

Fig. 8. Fluorescent micrographs of hMSCs grown on BPLH scaffold. (A) Cell proliferation of hMSCs (seeded at 10^4 cells/cm^2) on BPLH scaffold after 3 and 7 days of growth. (B) Fluorescence micrographs of hMSCs, seeded at a cellular density of 3×10^4 cells/cm^2, on BPLH scaffold after 2 weeks of growth stained with Crystal violet. Scale bars are of 100, 50 and 20 µm for Mag. 10X, 20X and 40X. (C) Fluorescent micrographs of hMSCs after 2 weeks of growth following nuclei staining with Hoechst 33,342. Scale bars are of 50 µm and 20 µm. (D) Confocal fluorescence micrographs of hMSCs after 2 weeks of growth stained with crystal violet and (E) superimposition of brightfield and confocal micrographs. Scale bars are of 20 µm. (For interpretation of the references to color in this figure legend, the reader is referred to the Web version of this article.)

functionalization of the biomaterial relevant for potential biomedical applications. Our results are also in agreement with other previous studies on bioplastics obtained from radicchio that had antioxidant properties linked to the presence of anthocyanins characteristic of this vegetable [59]. All these properties of the BPLH can be responsible of its scaffolding property observed for both NHDFs and hMSCs.

NHDFs grown on BPLH were able to express α-SMA, which is a protein important for the morphological and functional characteristics of smooth muscle and essential to wound contraction [63,64]. Several studies have demonstrated that dermal fibroblasts play a crucial role in repairing processes. In the injured region they can differentiate into myofibroblasts that is a highly contractile phenotype and thus be involved in wound closure [65–68]. Myofibroblasts play a key role in this process and are responsible for cell-mediated matrix contraction [69,70]. Myofibroblasts at the wound site are able to reduce the initial size of the wound through a contraction of their actin cytoskeleton, thereby promoting the tissue repair [71]. Moreover, the intrinsic presence of the phytochemicals, such as polyphenols, in the BPLH may also play an important role improving the fibroblasts proliferation and the wound healing as already demonstrated in case of several plant extracts [72].

The immunofluorescence analysis demonstrated also the presence of a spindle morphology of the hMSCs with many cell-cell interactions after several weeks of growth indicating a possible application of the handy BPLH (see the video 2S) as scaffold for the stem cells growth. Although more studies are needed to elucidate the effects of this new biomaterial on stem cell growth and differentiation and to have a translation in food and medicine, these studies suggest a new approach of valorization of vegetable-wastes and bioplastics to develop cell-scaffold systems for producing both handy and naturally functionalized patches of normal dermal and stem cells for tissue repair and for *in vitro* production of new cell-based future food.

Supplementary video related to this article can be found at https://doi.org/10.1016/j.biomaterials.2022.121984

Credit author statement

Silvia Buonvino Methodology, Investigation, Data curation, Writing- Reviewing and Editing; **Matteo Ciocci**: Visualization, Investigation, Validation; **Francesca Nanni:** Methodology, Data curation; **Ilaria Cacciotti:** Methodology, Data curation, Writing- Reviewing and Editing; **Sonia Melino:** Conceptualization, Visualization, Investigation, Methodology, Data curation, Supervision, Writing- Original draft preparation; Writing- Reviewing and Editing.

Declaration of competing interest

The authors declare that they have no known competing financial interests or personal relationships that could have appeared to influence the work reported in this paper.

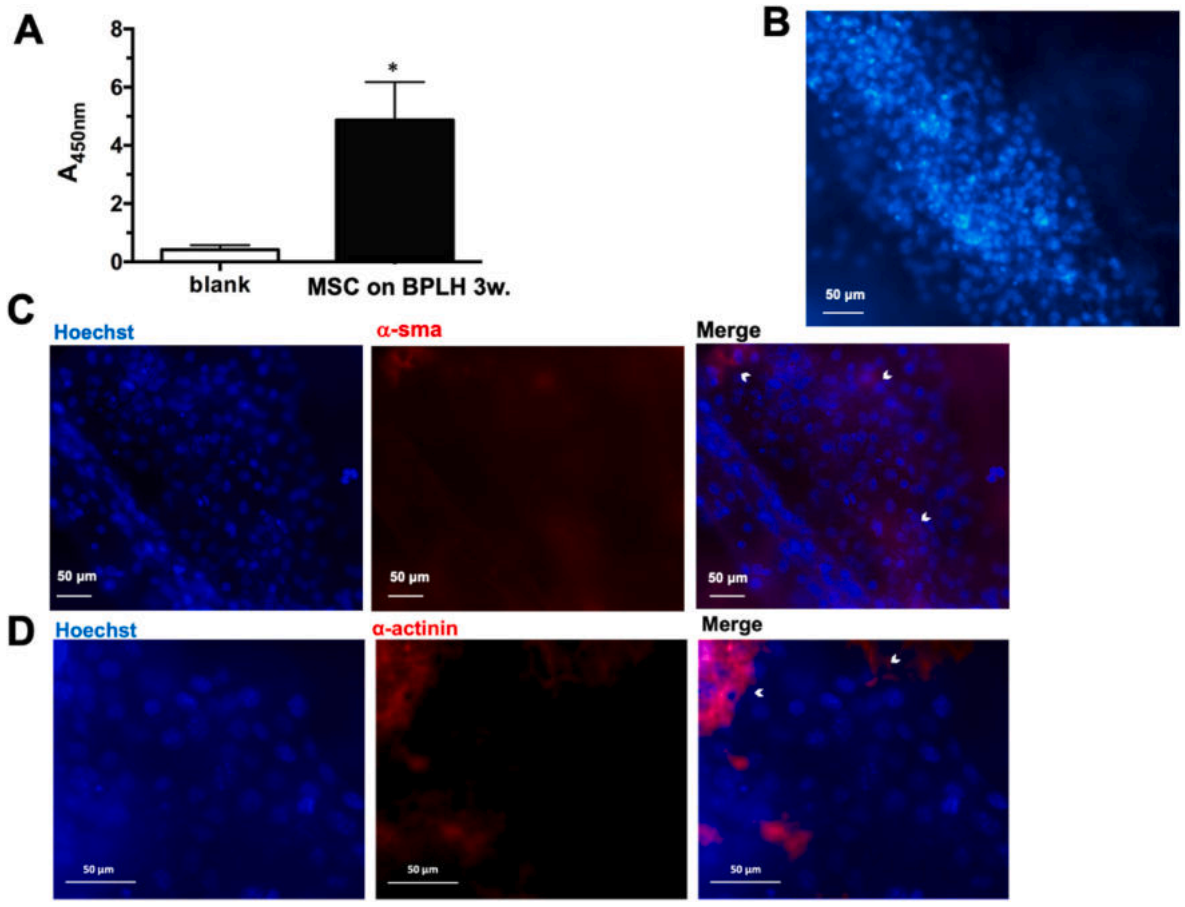

Fig. 9. BPLH scaffold used for long-growth of hMSCs. (A) Cell proliferation of hMSCs on BPLH scaffold after 3 weeks of growth. (B) (C) and (D) Fluorescence micrographs of hMSCs after 3 weeks of growth, nuclei are stained in blue with Hoechst 33,342, while α-SMA and α-actinin are stained in red. Scale bars are of 50 µm *p value $\leq$ 0.05. The arrows indicate the regions rich of α-SMA and α-actinin, respectively. (For interpretation of the references to color in this figure legend, the reader is referred to the Web version of this article.)

Data availability

Data will be made available on request.

Acknowledgements

We thank prof. P. Di Nardo to give us the human cardiac resident MSC line and Noemi Labbate for her technical support in some experiments.

Appendix A. Supplementary data

Supplementary data to this article can be found online at https://doi.org/10.1016/j.biomaterials.2022.121984.

References

[1] Z. Liu, M. Tang, J. Zhao, R. Chai, J. Kang, Looking into the future: toward advanced 3D biomaterials for stem-cell-based regenerative medicine, Adv. Mater. 30 (2018), 1705388, https://doi.org/10.1002/adma.201705388.

[2] G.M. Cunniffe, P.J. Díaz-Payno, E.J. Sheehy, S.E. Critchley, H.V. Almeida, P. Pitacco, S.F. Carroll, O.R. Mahon, A. Dunne, T.J. Levingstone, C.J. Moran, R. T. Brady, F.J. O'Brien, P.A.J. Brama, D.J. Kelly, Tissue-specific extracellular matrix scaffolds for the regeneration of spatially complex musculoskeletal tissues, Biomaterials 188 (2019) 63–73, https://doi.org/10.1016/j.biomaterials.2018.09.044.

[3] H. Abdelrazik, E. Giordano, G. Barbanti Brodano, C. Griffoni, E. De Falco, A. Pelagalli, Substantial overview on mesenchymal stem cell biological and physical properties as an opportunity in translational medicine, Int. J. Mol. Sci. 20 (2019), https://doi.org/10.3390/ijms20215386.

[4] W.B. Swanson, M. Omi, Z. Zhang, H.K. Nam, Y. Jung, G. Wang, P.X. Ma, N. E. Hatch, Y. Mishina, Macropore design of tissue engineering scaffolds regulates mesenchymal stem cell differentiation fate, Biomaterials 272 (2021), 120769, https://doi.org/10.1016/j.biomaterials.2021.120769.

[5] T. Biswal, S.K. BadJena, D. Pradhan, Sustainable biomaterials and their applications: a short review, Mater. Today Proc. 30 (2020) 274–282, https://doi.org/10.1016/j.matpr.2020.01.437.

[6] V. Wankhade, Chapter 6 - Animal-derived biopolymers in food and biomedical technology, in: K. Pal, I. Banerjee, P. Sarkar, D. Kim, W.-P. Deng, N.K. Dubey, K. Majumder (Eds.), Biopolymer-Based Formulations, Elsevier, 2020, pp. 139–152, https://doi.org/10.1016/B978-0-12-816897-4.00006-0.

[7] M.A. Elkodous, H.M. El-Husseiny, G.S. El-Sayyad, A.H. Hashem, A.S. Doghish, D. Elfadil, Y. Radwan, H.M. El-Zeiny, H. Bedair, O.A. Ikhdair, H. Hashim, A. M. Salama, H. Alshater, A.A. Ahmed, M.G. Elsayed, M. Nagy, N.Y. Ali, M. Elahmady, A.M. Kamel, M.A. Elkodous, I. Maallem, M.B.S. Kaml, N. Nasser, A. A. Nouh, F.M. Safwat, M.M. Alshal, S.K. Ahmed, T. Nagib, F.M. El-sayed, M. Almahdi, Y. Adla, N.T. ElNashar, A.M. Hussien, A.S. Salih, S.A. Mahmoud, S. Magdy, D.I. Ahmed, F.M.S. Hassan, N.A. Edward, K.S. Milad, S.R. Halasa, M. M. Arafa, A. Hegazy, G. Kawamura, W.K. Tan, A. Matsuda, Recent advances in waste-recycled nanomaterials for biomedical applications: waste-to-wealth, Nanotechnol. Rev. 10 (2021) 1662–1739, https://doi.org/10.1515/ntrev-2021-0099.

[8] D. Klemm, D. Schumann, U. Udhardt, S. Marsch, Bacterial synthesized cellulose — artificial blood vessels for microsurgery, Prog. Polym. Sci. 26 (2001) 1561–1603, https://doi.org/10.1016/S0079-6700(01)00021-1.

[9] A. Svensson, E. Nicklasson, T. Harrah, B. Panilaitis, D.L. Kaplan, M. Brittberg, P. Gatenholm, Bacterial cellulose as a potential scaffold for tissue engineering of cartilage, Biomaterials 26 (2005) 419–431, https://doi.org/10.1016/j.biomaterials.2004.02.049.

[10] L.G. Griffith, M.A. Swartz, Capturing complex 3D tissue physiology in vitro, Nat. Rev. Mol. Cell Biol. 7 (2006) 211–224, https://doi.org/10.1038/nrm1858.

[11] H. Page, P. Flood, E.G. Reynaud, Three-dimensional tissue cultures: current trends and beyond, Cell Tissue Res. 352 (2013) 123–131, https://doi.org/10.1007/s00441-012-1441-5.

[12] J.R. Gershlak, S. Hernandez, G. Fontana, L.R. Perreault, K.J. Hansen, S.A. Larson, B.Y.K. Binder, D.M. Dolivo, T. Yang, T. Dominko, M.W. Rolle, P.J. Weathers,

F. Medina-Bolivar, C.L. Cramer, W.L. Murphy, G.R. Gaudette, Crossing kingdoms: using decellularized plants as perfusable tissue engineering scaffolds, Biomaterials 125 (2017) 13–22, https://doi.org/10.1016/j.biomaterials.2017.02.011.
[13] R. Cancelliere, F. Zurlo, L. Micheli, S. Melino, Vegetable waste scaffolds for 3D-stem cell proliferating systems and low cost biosensors, Talanta 223 (2021), 121671, https://doi.org/10.1016/j.talanta.2020.121671.
[14] D.J. Modulevsky, C. Lefebvre, K. Haase, Z. Al-Rekabi, A.E. Pelling, Apple derived cellulose scaffolds for 3D mammalian cell culture, PLoS One 9 (2014) 1–10, https://doi.org/10.1371/journal.pone.0097835.
[15] D.J. Modulevsky, C.M. Cuerrier, A.E. Pelling, Biocompatibility of subcutaneously implanted plant-derived cellulose biomaterials, PLoS One 11 (2016) 1–19, https://doi.org/10.1371/journal.pone.0157894.
[16] J.T. Holmes, Z. Jaberansari, W. Collins, M.L. Latour, D.J. Modulevsky, A.E. Pelling, Homemade bread: repurposing an ancient technology for in vitro tissue engineering, Biomaterials 280 (2022), 121267, https://doi.org/10.1016/j.biomaterials.2021.121267.
[17] C. Demitri, M.G. Raucci, A. Giuri, V.M. De Benedictis, D. Giugliano, P. Calcagnile, A. Sannino, L. Ambrosio, Cellulose-based porous scaffold for bone tissue engineering applications: assessment of hMSC proliferation and differentiation, J. Biomed. Mater. Res. 104 (2015) 726–733, https://doi.org/10.1002/jbm.a.35611.
[18] J. Lee, H. Jung, N. Park, S.-H. Park, J.H. Ju, Induced osteogenesis in plants decellularized scaffolds, Sci. Rep. 9 (2019), 20194, https://doi.org/10.1038/s41598-019-56651-0.
[19] M.L. Latour, M. Tarar, R.J. Hickey, C.M. Cuerrier, I. Catelas, A.E. Pelling, Plant-derived cellulose scaffolds for bone tissue engineering, BioRxiv (2020), https://doi.org/10.1101/2020.01.15.906677.
[20] R. Polak, E.M. Phillips, A. Campbell, Legumes: health benefits and culinary approaches to increase intake, Clin. Diabetes 33 (2015) 198–205, https://doi.org/10.2337/diaclin.33.4.198.
[21] World Health Organization, Healthy diet. https://www.who.int/news-room/fact-sheets/detail/healthy-diet, 2022 accessed 2022.
[22] C.A. Moreno-Valdespino, D. Luna-Vital, R.M. Camacho-Ruiz, L. Mojica, Bioactive proteins and phytochemicals from legumes: mechanisms of action preventing obesity and type-2 diabetes, Food Res. Int. 130 (2020), 108905, https://doi.org/10.1016/j.foodres.2019.108905.
[23] M. van de Noort, Chapter 10 - Lupin: an important protein and nutrient source, in: S.R. Nadathur, J.P.D. Wanasundara, L. Scanlin (Eds.), Sustainable Protein Sources, Academic Press, San Diego, 2017, pp. 165–183, https://doi.org/10.1016/B978-0-12-802778-3.00010-X.
[24] S. Shrestha, L. van 't Hag, V.S. Haritos, S. Dhital, Lupin proteins: structure, isolation and application, Trends Food Sci. Technol. 116 (2021) 928–939, https://doi.org/10.1016/j.tifs.2021.08.035.
[25] R.P. Hansen, Z. Czochanska, Composition of the lipids of lupin seed (*Lupinus angustifolius* L. var. "uniwhite"), J. Sci. Food Agric. 25 (1974) 409–415, https://doi.org/10.1002/jsfa.2740250409.
[26] E.A. El-Difrawi, B.J.F. Hudson, Identification and estimation of carotenoids in the seeds of four Lupinus species, J. Sci. Food Agric. 30 (1979) 1168–1170, https://doi.org/10.1002/jsfa.2740301209.
[27] J. Rowe, G. Hargreave, Nutritive value of lupin hulls, Proc. Aust. Soc. Anim. Prod. 17 (1988) 463.
[28] A.J. Evans, The carbohydrates of lupins, composition and uses, in: M. Dracup, J. Palta (Eds.), Proc. of the 1st Austral, Lupin Tech. Symp., Perth, Australia, 1994, pp. 110–114.
[29] E. Lampart-Szczapa, J. Korczak, M. Nogala-Kalucka, R. Zawirska-Wojtasiak, Antioxidant properties of lupin seed products, Food Chem. 83 (2003) 279–285, https://doi.org/10.1016/S0308-8146(03)00091-8.
[30] S. Wang, S. Errington, H. Yap, Studies on Carotenoids from Lupin Seeds, International Lupin Association, 2008, 0–86476.
[31] M. Duranti, P. Morazzoni, Nutraceutical properties of lupin seed proteins. A great potential still waiting for full exploitation, Agro, Food Ind. Hi Technol. 22 (2011) 20–23.
[32] A.A. Hamama, H.L. Bhardwaj, Phytosterols, triterpene alcohols, and phospholipids in seed oil from white lupin, JAOCS (J. Am. Oil Chem. Soc.) 81 (2004) 1039–1044, https://doi.org/10.1007/s11746-004-1019-z.
[33] J.B. Nikiéma, R. Vanhaelen-Fastré, M. Vanhaelen, J. Fontaine, C. De Graef, M. Heenen, Effects of antiinflammatory triterpenes isolated from Leptadenia hastata latex on Keratinocyte Proliferation, Phytother Res. 15 (2001) 131–134, https://doi.org/10.1002/ptr.700.
[34] P. Msika, A. Piccirilli, N. Piccardi, Use of a Cosmetic of Pharmaceutical Composition, Comprising a Lupeol-rich Extract as an Active Ingredient for Stimulating the Synthesis of Heat Shock Proteins, 2006. Patent USPTO #: 20060216249 – Class: 424058000.
[35] K. Hata, K. Hori, S. Takahashi, Role of p38 MAPK in lupeol-induced B16 2F2 mouse melanoma cell differentiation, J. Biochem. 134 (2003) 441–445, https://doi.org/10.1093/jb/mvg162.
[36] M. Saleem, F. Afaq, V.M. Adhami, H. Mukhtar, Lupeol modulates NF-kappaB and PI3K/Akt pathways and inhibits skin cancer in CD-1 mice, Oncogene 23 (2004) 5203–5214, https://doi.org/10.1038/sj.onc.1207641.
[37] G.F. Nsonde Ntandou, J.T. Banzouzi, B. Mbatchi, R.D.G. Elion-Itou, A.W. Etou-Ossibi, S. Ramos, F. Benoit-Vical, A.A. Abena, J.M. Ouamba, Analgesic and anti-inflammatory effects of Cassia siamea Lam. stem bark extracts, J. Ethnopharmacol. 127 (2010) 108–111, https://doi.org/10.1016/j.jep.2009.09.040.
[38] E.J. Blain, A.Y. Ali, V.C. Duance, Boswellia frereana (frankincense) suppresses cytokine-induced matrix metalloproteinase expression and production of pro-inflammatory molecules in articular cartilage, Phytother Res. 24 (2010) 905–912, https://doi.org/10.1002/ptr.3055.
[39] A.M. Pedernera, T. Guardia, C.E. Guardia Calderón, A.E. Rotelli, N.E. de la Rocha, J.R. Saad, M.A. Lopez Verrilli, S. Garcia Aseff, L.E. Pelzer, Anti-inflammatory effect of Acacia visco extracts in animal models, Inflammopharmacology 18 (2010) 253–260, https://doi.org/10.1007/s10787-009-0028-6.
[40] M. Saleem, I. Murtaza, R.S. Tarapore, Y. Suh, V.M. Adhami, J.J. Johnson, I. A. Siddiqui, N. Khan, M. Asim, B.B. Hafeez, M.T. Shekhani, B. Li, H. Mukhtar, Lupeol inhibits proliferation of human prostate cancer cells by targeting β-catenin signaling, Carcinogenesis 30 (2009) 808–817, https://doi.org/10.1093/carcin/bgp044.
[41] A. Petronelli, G. Pannitteri, U. Testa, Triterpenoids as new promising anticancer drugs, Anti Cancer Drugs 20 (2009) 880–892, https://doi.org/10.1097/CAD.0b013e328330fd90.
[42] M.N. Laszczyk, Pentacyclic triterpenes of the lupane, oleanane and ursane group as tools in cancer therapy, Planta Med. 75 (2009) 1549–1560.
[43] A. Marquez-Martin, R.D.L. Puerta, A. Fernandez-Arche, V. Ruiz-Gutierrez, P. Yaqoob, Modulation of cytokine secretion by pentacyclic triterpenes from olive pomace oil in human mononuclear cells, Cytokine 36 (2006) 211–217, https://doi.org/10.1016/j.cyto.2006.12.007.
[44] V. Singleton, J. Rossi, Colorimetry of total phenolic compounds with phosphomolybdic-phosphotungstic acid reagents, Am. J. Enol. Vitic. 16 (1965) 144–158.
[45] M. Ciocci, I. Cacciotti, D. Seliktar, S. Melino, Injectable silk fibroin hydrogels functionalized with microspheres as adult stem cells-carrier systems, Int. J. Biol. Macromol. 108 (2018) 960–971, https://doi.org/10.1016/j.ijbiomac.2017.11.013.
[46] A. Forte, B. Rinaldi, L. Sodano, L. Berrino, F. Rossi, M. Finicelli, M. Grossi, G. Cobellis, C. Botti, M. De Feo, P. Santè, U. Galderisi, M. Cipollaro, Stem cell therapy for arterial restenosis: potential parameters contributing to the success of bone marrow-derived mesenchymal stromal cells, Cardiovasc. Drugs Ther. 26 (2012) 9–21, https://doi.org/10.1007/s10557-011-6359-8.
[47] F. Denizot, R. Lang, Rapid colorimetric assay for cell growth and survival: modifications to the tetrazolium dye procedure giving improved sensitivity and reliability, J. Immunol. Methods 89 (1986) 271–277, https://doi.org/10.1016/0022-1759(86)90368-6.
[48] M. Koyanagi, S. Kawakabe, Y. Arimura, A comparative study of colorimetric cell proliferation assays in immune cells, Cytotechnology 68 (2016) 1489–1498, https://doi.org/10.1007/s10616-015-9909-2.
[49] I.S. Bayer, S. Guzman-Puyol, J.A. Heredia-Guerrero, L. Ceseracciu, F. Pignatelli, R. Ruffilli, R. Cingolani, A. Athanassiou, Direct transformation of edible vegetable waste into bioplastics, Macromolecules 47 (2014) 5135–5143, https://doi.org/10.1021/ma5008557.
[50] A.M. Raspolli Galletti, A. D'Alessio, D. Licursi, C. Antonetti, G. Valentini, A. Galia, N. Nassi o Di Nasso, Midinfrared FT-IR as a tool for monitoring herbaceous biomass composition and its conversion to furfural, J. Spectrosc. (2015), 719042, https://doi.org/10.1155/2015/719042, 2015.
[51] A.M. Ritcey, K.R. Holme, D.G. Gray, Cholesteric properties of cellulose acetate and triacetate in trifluoroacetic acid, Macromolecules 21 (1988) 2914–2917, https://doi.org/10.1021/ma00188a003.
[52] M.M. Lucas, F. Stoddard, P. Annicchiarico, J. Frias, C. Martinez-Villaluenga, D. Sussmann, M. Duranti, A. Seger, P. Zander, J. Pueyo, The future of lupin as a protein crop in Europe, Front. Plant Sci. 6 (2015). https://www.frontiersin.org/article/10.3389/fpls.2015.00705.
[53] J.C.M. Wolkers – Rooijackers, M.F. Endika, E.J. Smid, Enhancing vitamin B12 in lupin tempeh by in situ fortification, LWT 96 (2018) 513–518, https://doi.org/10.1016/j.lwt.2018.05.062.
[54] A. Alcorta, A. Porta, A. Tarrega, M.D. Alvarez, M.P. Vaquero, Foods for plant-based diets: challenges and innovations, Foods 10 (2021), https://doi.org/10.3390/foods10020293.
[55] S. Iravani, A.K. Shukla, Plant protein-based nanoparticles and their biomedical applications, in: A. Husen, M. Iqbal (Eds.), Nanomaterials and Plant Potential, Springer International Publishing, Cham, 2019, pp. 177–191, https://doi.org/10.1007/978-3-030-05569-1_6.
[56] J. Lacombe, A.F. Harris, R. Zenhausern, S. Karsunsky, F. Zenhausern, Plant-based scaffolds modify cellular response to drug and radiation exposure compared to standard cell culture models, Front. Bioeng. Biotechnol. 8 (2020), https://doi.org/10.3389/fbioe.2020.00932.
[57] A.C. Bilirgen, M. Toker, S. Odabb, A.K. Yetisen, B. Garipcan, S. Tasoglu, Plant-based scaffolds in tissue engineering, ACS Biomat. Sci. Eng. 7 (2021), 926-938,doi: 10.1021/acsbiomaterials.0c01527.
[58] R. Reshmy, E. Philip, P.H. Vaisakh, S. Raj, S.A. Paul, A. Madhavan, R. Sindhu, P. Binod, R. Sirohi, A. Pugazhendhi, A. Pandey, Development of an eco-friendly biodegradable plastic from jack fruit peel cellulose with different plasticizers and Boswellia serrata as filler, Sci. Total Environ. 767 (2021), 144285, https://doi.org/10.1016/j.scitotenv.2020.144285.
[59] G. Perotto, L. Ceseracciu, R. Simonutti, U.C. Paul, S. Guzman-Puyol, T.-N. Tran, I. S. Bayer, A. Athanassiou, Bioplastics from vegetable waste via an eco-friendly water-based process, Green Chem. 20 (2018) 894–902, https://doi.org/10.1039/C7GC03368K.
[60] M.F.M.A. Zamri, R. Bahru, R. Amin, M.U. Aslam Khan, S.I.A. Razak, S.A. Hassan, M.R.A. Kadir, N.H.M. Nayan, Waste to health: a review of waste derived materials for tissue engineering, J. Clean. Prod. 290 (2021), 125792, https://doi.org/10.1016/j.jclepro.2021.125792.
[61] S. Jana, P. Das, J. Mukherjee, D. Banerjee, P.R. Ghosh, P. Kumar Das, R. N. Bhattacharya, S.K. Nandi, Waste-derived biomaterials as building blocks in the

biomedical field, J. Mater. Chem. B. 10 (2022) 489–505, https://doi.org/10.1039/D1TB02125G.
[62] K.S. Ganesh, A. Sridhar, S. Vishali, Utilization of fruit and vegetable waste to produce value-added products: conventional utilization and emerging opportunities-A review, Chemosphere 287 (2022), 132221, https://doi.org/10.1016/j.chemosphere.2021.132221.
[63] N. Kakudo, S. Kushida, K. Suzuki, T. Ogura, P.V. Notodihardjo, T. Hara, K. Kusumoto, Effects of transforming growth factor-beta1 on cell motility, collagen gel contraction, myofibroblastic differentiation, and extracellular matrix expression of human adipose-derived stem cell, Hum. Cell 25 (2012) 87–95, https://doi.org/10.1007/s13577-012-0049-0.
[64] M. Eldardiri, Y. Martin, J. Roxburgh, D.J. Lawrence-Watt, J.R. Sharpe, Wound contraction is significantly reduced by the use of microcarriers to deliver keratinocytes and fibroblasts in an in vivo pig model of wound repair and regeneration, Tissue Eng. 18 (2012) 587–597, https://doi.org/10.1089/ten.tea.2011.0258.
[65] S. Barrientos, O. Stojadinovic, M.S. Golinko, H. Brem, M. Tomic-Canic, Perspective article: growth factors and cytokines in wound healing, Wound Repair Regen. 16 (2008) 585–601, https://doi.org/10.1111/j.1524-475X.2008.00410.x.
[66] C. Vittorazzi, D.C. Endringer, T.U. de Andrade, R. Scherer, M. Fronza, Antioxidant, antimicrobial and wound healing properties of Struthanthus vulgaris, Pharmaceut. Biol. 54 (2016) 331–337, https://doi.org/10.3109/13880209.2015.1040515.
[67] J.M. Reinke, H. Sorg, Wound repair and regeneration, Eur. Surg. Res. 49 (2012) 35–43, https://doi.org/10.1159/000339613.
[68] S.A. Eming, P. Martin, M. Tomic-Canic, Wound repair and regeneration: mechanisms, signaling, and translation, Sci. Transl. Med. 6 (2014) 265sr6, https://doi.org/10.1126/scitranslmed.3009337, 265sr6.
[69] L. Follonier Castella, G. Gabbiani, C.A. McCulloch, B. Hinz, Regulation of myofibroblast activities: calcium pulls some strings behind the scene, Exp. Cell Res. 316 (2010) 2390–2401, https://doi.org/10.1016/j.yexcr.2010.04.033.
[70] G. Dabiri, D.A. Tumbarello, C.E. Turner, L. Van De Water, Hic-5 promotes the hypertrophic scar myofibroblast phenotype by regulating the TGF-β1 autocrine loop, J. Invest. Dermatol. 128 (2008) 2518–2525, https://doi.org/10.1038/jid.2008.90.
[71] J.J. Tomasek, G. Gabbiani, B. Hinz, C. Chaponnier, R.A. Brown, Myofibroblasts and mechano-regulation of connective tissue remodelling, Nat. Rev. Mol. Cell Biol. 3 (2002) 349–363, https://doi.org/10.1038/nrm809.
[72] R. Addis, S. Cruciani, S. Santaniello, E. Bellu, G. Sarais, C. Ventura, M. Maioli, G. Pintore, Fibroblast proliferation and migration in wound healing by phytochemicals: evidence for a novel synergic outcome, Int. J. Med. Sci. 17 (2020) 1030–1042, https://doi.org/10.7150/ijms.43986.

ELSEVIER

News

Plant waste promises biocompatible bioplastics

Reprocessing vegetable waste is emerging as a promising route to useful biomaterials for biomedicine and the food industry. New approaches to regenerative medicine and tissue engineering require biocompatible scaffolds to support the adhesion, proliferation, and differentiation of stem cells into replacement tissue. Biowaste could offer a cheap and abundant, as well as environmentally friendly, feedstock for such biomaterials. Recently, researchers from the University of Rome Tor Vergata have created two types of scaffold from the hull of the lupin plant (*Lupinus albus* L.) for the growth of human cells [Buonvino et al., Biomaterials (2023) doi: https://doi.org/10.1016/j.biomaterials.2022.121984].

The lupin has several potential health benefits and is becoming a major legume crop, particularly in environmentally stressed regions with low annual rainfall or poor soil. The hulls contain most of the plant's fibers, mainly cellulose and hemicellulose, as well as natural antioxidants. The first scaffold is produced by treating the hulls with ethanol for 24 hours, before washing and lyophilizing. The dried material can be stored for weeks and rehydrated in PBS whenever required. The lupin-derived scaffold has a high cellulose content and contains beneficial phytochemicals. Moreover, the material shows good adhesion and proliferation of human mesenchymal stem cells (hMSCs).

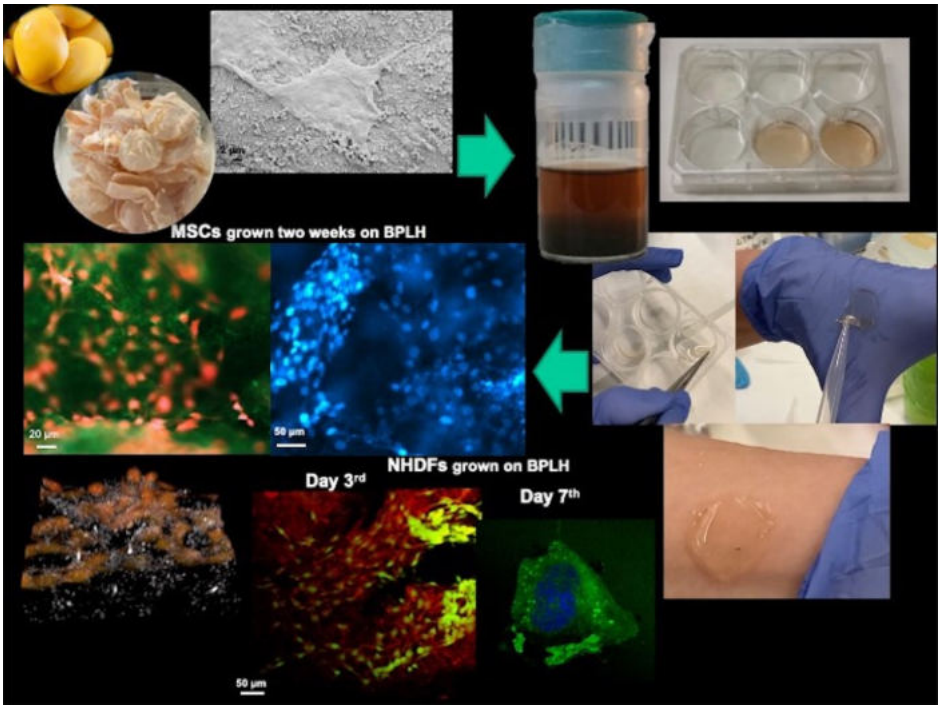

Production, characterization, and usage of biomaterial and BPLH bioplastic based on lupin hulls.

A second scaffold material was produced by incubating dried, finely crushed hulls in trifluoracetic acid (TFA) for 48 hours. This approach has been used previously to produce bioplastics from a range of different vegetal species from parsley and spinach stalks to rice and cocoa husks. Like the other scaffold material, the 'BPLH' bioplastic shows good adhesion and proliferation of hMSCs and fibroblasts, as well as the initial signs of muscle cell differentiation. BPLH can absorb considerable amounts of water rapidly and is more stable than other vegetable-derived bioplastics.

The bioplastic's flexibility and smooth surface make it potentially suitable for biomedicine applications, such as cell culture or wound healing, or food packaging, the researchers suggest.

"Our results show a possible valorization of waste-derived bioplastics to develop low-cost, naturally functionalized patches for regenerative medicine and the production of cell-based food," adds Sonia Melino,

who led the work. "This versatile lupin hull biomaterial gives new life and value to extensively produced vegetable waste."

The team now plan to work on improving the fabrication, mechanical and electric properties of the BPLH material and exploit its autofluorescence properties in biosensing applications.

Cordelia Sealy

1369-7021/https://doi.org/10.1016/j.mattod.2023.03.012

Cellulose ink makes printing 3D wearable electronics easy

Researchers from KTH Royal Institute of Technology in Sweden have developed a conductive cellulose-based ink for printing three-dimensional (3D) stretchable wearable electronics that is cheaper and less energy intensive to produce [Jain et al., Appl. Mater. Today (2023) doi:https://doi.org/10.1016/j.apmt.2022.101703].

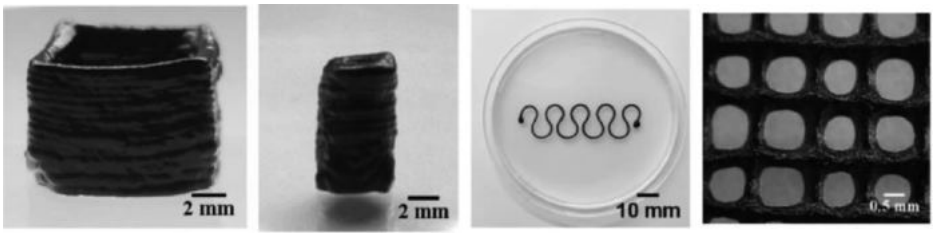

Optical photographs of printed 3D and 2D patterns of conductive ink (from left to right) in a 20-layered hollow cube, a hollow cylinder, a 5-layered serpentine pattern, and a 5-layered mesh structure.

Bio-based electronics are of growing interest for wearable applications in energy storage, energy harvesting or biomedicine. But the conductive polymers, such as poly(3,4-ethylene dioxythiophene) (PEDOT) or poly(styrene sulfonate) (PSS), that are an essential component often require doping to increase conductivity, involving the use of harsh organic solvents or additives.

"[Our] motivation was to decrease the amount of conductive polymer in the ink because it is very expensive," explains first author of the study, Karishma Jain.

Moreover, while nanocellulose is often used in bio-based inks to modulate mechanical properties, its preparation is energy intensive and time consuming. Instead, the ink developed by Lars Wågberg's team based on PEDOT:PSS uses a form of cellulose known as dialcohol cellulose (DALC), where chemical modification opens the chain structure of the fibers.

"The use of macroscopic fibers is a crucial step since it simplifies the preparation of the ink, [avoiding] the energy intensive preparation of nanocellulose while still providing good rheological properties" adds Jain.

Like pearls on a necklace, polymer particles of PEDOT:PSS are supported by the DALC fibers, encouraging conformation change in the polymer chains and phase separation, which boost conductivity. When mixed with a plasticizer, the resulting DALC-PEDOT:PSS ink has the ideal viscoelastic properties for direct-ink writing in a 3D bioprinter.

"[The] ink formulation shows good conductive properties at less than 50 wt. % conducting polymer and without any harmful organic additives," points out Jain.

Reducing the amount of conductive polymer needed reduces costs, while the absence of harmful organic species makes fabrication easier. Using the novel ink, the researchers printed water-stable, stretchable, highly conductive structures with excellent electrochemical performance for wearable supercapacitors and biopotential monitoring devices for electrocardiography (ECG) and electromyography (EMG) measurements. The researchers believe that the work represents the first extrudable, modified cellulose fiber based, 3D printable conductive bio-ink that does not require the nanofibrillation of cellulose.

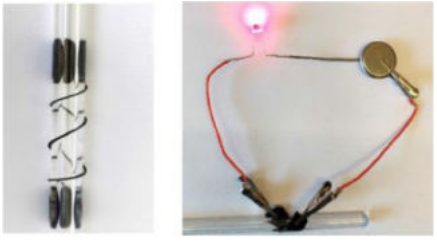

Photograph of a printed serpentine pattern (left) and film wrapped around a glass rod (radius of 3 mm) with glowing LED light.

"The material can be used in printed electronics," says Jain, "[and] bio-based conductive coatings on implantable bioelectronic devices as an interface between the body and the implanted device."

The team now hope to improve the adhesive and conductive properties of the composite to reduce production costs further.

Cordelia Sealy

1369-7021/https://doi.org/10.1016/j.mattod.2023.03.013

Low-energy approach to cleaning dirty water

With accessing clean water being increasingly difficult due to population rise and greater contamination of freshwater sources, researchers at Princeton University have developed a porous solar absorber gel for water purification inspired by the loofah sponge. Their sunlight-powered hydrogel absorbs polluted water at room temperature before quickly releasing purified water when heated, enough for a person's daily requirements.

While other sunlight-driven evaporation processes can purify water, they are less effective when it is cloudy, and tend to produce only a few gallons of water per day. One approach has been to use temperature-responsive hydrogels such as poly(N-isopropyl acrylamide) (PNIPAm), which switch from absorbing water at cooler temperatures to repelling it on being heated. However, standard PNIPAm gels can't produce clean water sufficiently quickly due to their closed-off pores.

As reported in *ACS Central Science* [Xu et al., ACS Cent. Sci. (2023) doi:https://doi.org/10.1021/acscentsci.2c01245], this led the team to investigate copying the